

## Structure and energy of point defects in TiC: An *ab initio* study

Weiwei Sun,<sup>1,2,\*</sup> Hossein Ehteshami,<sup>1</sup> and Pavel A. Korzhavyi<sup>1,3</sup>

<sup>1</sup>*Department of Material Science and Engineering, KTH-Royal Institute of Technology, SE-100 44 Stockholm, Sweden*

<sup>2</sup>*Department of Physics and Astronomy, Uppsala University, Box 516, SE-751 20 Uppsala, Sweden*

<sup>3</sup>*Institute of Metal Physics, Ural Division of the Russian Academy of Sciences, 620219 Ekaterinburg, Russia*

(Received 12 December 2014; revised manuscript received 2 April 2015; published 24 April 2015)

We employ first-principles calculations to study the atomic and electronic structure of various point defects such as vacancies, interstitials, and antisites in the stoichiometric as well as slightly off-stoichiometric  $\text{Ti}_{1-c}\text{C}_c$  (including both C-poor and C-rich compositions,  $0.49 \leq c \leq 0.51$ ). The atomic structure analysis has revealed that both interstitial and antisite defects can exist in split conformations involving dumbbells. To characterize the electronic structure changes caused by a defect, we introduce differential density of states (dDOS) defined as a local perturbation of the density of states (DOS) on the defect site and its surrounding relative to the perfect TiC. This definition allows us to identify the DOS peaks characteristic of the studied defects in several conformations. So far, characteristic defect states have been discussed only in connection with carbon vacancies. Here, in particular, we have identified dDOS peaks of carbon interstitials and dumbbells, which can be used for experimental detection of such defects in TiC. The formation energies of point defects in TiC are derived in the framework of a grand-canonical formalism. Among the considered defects, carbon vacancies and interstitials are shown to have, respectively, the lowest and the second-lowest formation energies. Their formation energetics are consistent with the thermodynamic data on the phase stability of nonstoichiometric TiC. A cluster type of point defect is found to be next in energy, a titanium [100] dumbbell terminated by two carbon vacancies.

DOI: [10.1103/PhysRevB.91.134111](https://doi.org/10.1103/PhysRevB.91.134111)

PACS number(s): 61.72.J-, 66.30.-h, 81.05.Je, 31.15.A-

### I. INTRODUCTION

Transition-metal (TM) carbides and nitrides combine properties typical of ceramics (high melting point, great hardness, good wear, and corrosion resistance) with the properties typical of metals (high electrical and thermal conductivity) [1,2]. This combination of properties makes TM carbides and nitrides highly suitable materials for cutting-tool applications [3,4]. Titanium carbide, TiC, is the best-studied case, and is often considered to be a prototype compound, of the whole family of cubic TM carbides and nitrides [5–9]. Titanium carbide is used for making hard coatings, as a hard phase in composite materials, and is also attractive for applications in catalysis [10] and in the aerospace industry [4,7].

TiC crystallizes in the NaCl-type structure with the ideal stoichiometric ratio (1:1) between the components. In practice, however, the full stoichiometry is difficult to reach, because carbon vacancies can be stably present in TiC (the fraction of vacant carbon sites may reach 50%) [11,12]. The nature of chemical bonding in TM carbides and their structural stability have been studied theoretically using *ab initio* calculations, concluding that the bonding in these compounds may be described as a mixture of covalent, ionic, and metallic types. A number of comprehensive reviews can be found [13–17]. The bonding in TiC is prevalently covalent near the stoichiometric composition [18–23], whereas at large deviations from stoichiometry (corresponding to a decreased carbon content) the metallic component of bonding becomes more pronounced [13,14]. This variation of chemical bonding with composition underlies the effect of carbon vacancies on the physical, chemical, and mechanical properties of titanium carbide [3,24–28].

Experimental studies using electron spectroscopy [29,30], electron diffraction [11], x-ray diffraction [31–33], and neutron scattering [34–36] have mostly been focused on the properties of carbon vacancies which are the most abundant point defects in substoichiometric  $\text{TiC}_{1-x}$ , where  $x$  is the site fraction of carbon vacancies. A limited amount of experimental information is available on the properties of other point defects in TiC. For instance, experimental evidence has been found for the trapping of positrons at vacant Ti sites in slightly substoichiometric polycrystalline TiC [37] and for the presence of interstitial carbon atoms in near-stoichiometric TiC thin films prepared by plasma deposition [38,39].

The situation with theoretical studies of point defects in TiC and related compounds is similar: The greatest attention and computational effort have been devoted to nonmetal vacancies. Nonmetal vacancies have been reported to induce so-called vacancy states in the pseudogap between the bonding and the antibonding states in the electronic structure of substoichiometric TiC and TiN [24–26]. Theoretical analyses based on the tight-binding (TB) approach have revealed the origins of stability of carbon vacancies in TiC [40,41]. Interaction and ordering of nonmetal vacancies in titanium carbonitride have been extensively studied using *ab initio*-based modeling approaches [42–45] to complement the systematic experimental studies of vacancy ordering in refractory carbides and nitrides.

Intrinsic point defects other than nonmetal vacancies in TiC and related compounds have been mostly neglected, partly due to their high formation energies [46,47]. However, a systematic *ab initio* study of intrinsic point defects has been undertaken [48], which included vacancies and interstitials (including split interstitial geometries), as well as their complexes. High migration barriers for the carbon-vacancy and titanium-vacancy exchanges in TiC have been computed [47,48]. While the calculated interactions between

\*Corresponding author: [provels8467@gmail.com](mailto:provels8467@gmail.com)

two identical point defects in TiC are mostly repulsive at close distances, strong binding between a metal vacancy and a carbon vacancy in TiC and ZrC has been found [48,49]. This interaction lowers the formation energy of a metal vacancy in the substoichiometric carbides by about 5 eV for the configuration where one metal vacancy is fully surrounded by six carbon vacancies [49].

In this paper, *ab initio* calculations based on density functional theory [50,51] are employed to study the structure and formation energies for an extended list of point defects in titanium carbide that includes titanium  $Va_{Ti}$  and carbon  $Va_C$  vacancies, titanium  $Ti_C$  and carbon  $C_{Ti}$  antisite defects, as well as titanium  $Ti_I$  and carbon  $C_I$  interstitials. For the antisites and interstitials, symmetric (site-centered) and asymmetric (off-center) positions have been considered, as well as conformations involving dumbbells (two atoms sharing a lattice site),  $Ti_D \equiv \{2Ti\}_{Ti}$  and  $C_D \equiv \{2C\}_C$ , in two orientations, [100] and [110]. A database of calculated properties (relaxed geometry, electronic structure, and defect formation energy) of these defects in near-stoichiometric TiC is thus obtained, which may be useful for atomistic and multiscale modeling, as well as for experimental characterization of point defects in titanium carbide. In this paper we use the calculated defect formation energies to make a qualitative analysis of constitutional and thermal point defects in TiC.

## II. COMPUTATIONAL METHODS

The electronic and atomic structure of native point defects in TiC, as well as their formation energies, were calculated using density functional theory (DFT) and the projector augmented wave (PAW) method [52,53], as implemented in the Vienna Ab-initio Simulation Package (VASP) [54–56]. The total energies of the pristine and defected TiC supercells were obtained in the generalized gradient approximation (GGA) using the PBE functional formulated by Perdew, Burke, and Ernzerhof [57]. Within PAW, the Ti-3*d*, Ti-4*s*, C-2*s*, and C-2*p* states were treated as valence states, while the Ti-3*s* and Ti-3*p* semicore states were kept frozen. A cutoff energy of 400 eV was used in all calculations. Such important parameters as the supercell size and the  $\mathbf{k}$ -point mesh density were already tested in a previous study [49]. It was found that a 216-site supercell with a  $5 \times 5 \times 5$  Monkhorst-Pack  $\mathbf{k}$ -point mesh was large enough to achieve acceptable precision. For the Brillouin zone integration, the first order of the Methfessel-Paxton method [58] with a 0.05-eV width was applied, in which the maximum entropy term value of 1 meV per atom had been achieved. In order to obtain accurate density of states (DOS), a much denser  $\mathbf{k}$ -point mesh ( $9 \times 9 \times 9$ ) was used together with the Gaussian smearing method and a width of 0.1 eV. The convergence criteria were set to be  $10^{-5}$  eV for the total energy and  $10^{-2}$  eV/Å for the forces. The ionic positions were allowed to relax in all cases.

## III. ATOMIC AND ELECTRONIC STRUCTURE OF POINT DEFECTS

In this section, the calculated changes in the atomic and electronic structure of TiC due to native point defects will be presented and discussed. For the purpose of plotting the

atomic structures, the VESTA package [59] has been exploited. When doing the calculations, we started our consideration with six basic point defect species in TiC in their simplest (symmetric) conformations: two kinds of vacancies,  $Va_C$  and  $Va_{Ti}$ , two antisite defects,  $Ti_C$  and  $C_{Ti}$ , and two interstitial atoms,  $Ti_I$  and  $C_I$ . By breaking the symmetry around each defect in several different ways, we checked whether an asymmetric conformation of this defect may be mechanically stable. An asymmetric form of carbon interstitial ( $C'_I$ ) has thus been identified. In addition, split interstitial and split antisite conformations involving dumbbells oriented along the  $\langle 100 \rangle$  and  $\langle 110 \rangle$  crystallographic directions have been found to be mechanically stable for both carbon and titanium. Our search for the stable and metastable conformations of point defects was simplified by the symmetry of the TiC crystal lattice, as well as by the fact that many of the conformations were known from a previous study [48]. In a general case, one would have to explore the potential energy landscape for every defect, by sampling the configurational space using either a regular grid [60] or an automated technique such as metadynamics [61], to locate the energy minima.

Information about the electronic structure can provide useful insights into the origins of mechanical stability or instability of various point defects and point-defect arrangements. Also, if a defect forms very characteristic electron states (such as defect levels in semiconductors), these states can be used to detect the presence of the defect in the material and even to quantify the defect concentration, by spectroscopic methods. As mentioned in the Introduction, the instructive and clear electronic structure data for point defects (other than carbon vacancies) in TiC are lacking. The electronic structure data obtained in this work indicate that such point defects as carbon interstitials or dumbbells in TiC do form detectable electron states in the forbidden energy regions. This result enables spectroscopic studies of these defects which, according to our analysis of total energies presented in Sec. IV C, can be formed thermally or produced by irradiation in TiC.

When the defects are modeled using large supercells, a direct comparison of the total DOS of a defect-bearing supercell with that of pristine TiC does not allow to clearly see the characteristic peaks of the defects, as has been discussed previously [48]. Therefore, we construct a differential density of states (dDOS),  $\Delta n_s(E)$ , defined as the sum of projected DOS  $n_{i_s}(E)$  on sites  $i_s$  ( $s = Ti, C$ ) in the region perturbed by defect  $\alpha$  (the perturbed region is chosen to include the defect site and two coordination shells of atoms around it) *minus* the reference DOS  $n_{0,s}(E)$  projected on the Ti and C sites situated as far as possible from the defect site in the same supercell:

$$\Delta n_s(E) = \sum_{i_s=1}^{N_s^\alpha} [n_{i_s}(E) - n_{0,s}(E)]. \quad (1)$$

Here  $N_s^\alpha$  are the numbers of Ti and C atoms included in the perturbed region, and  $E$  is the electron energy relative to the Fermi level  $E_F$ . Under such a definition, the states that are created as a result of formation of a defect (so-called defect states) will be seen as positive peaks at a certain energy, whereas the host states that are annihilated upon the formation of the defect will be seen as negative peaks of the dDOS. The

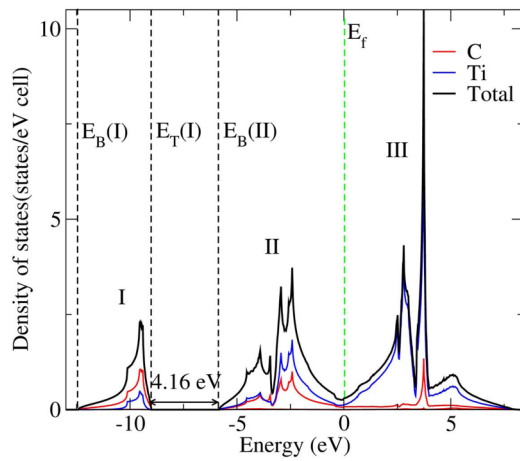


FIG. 1. (Color online) Calculated total DOS (black line) and site-projected DOS of pristine TiC. The Ti states are shown in blue and those of C in red. The energy is given relative to the Fermi level  $E_F$  (green dashed line). Vertical black dashed lines indicate the edges (top  $E_T$  or bottom  $E_B$ ) of the lower (region I) and the upper (regions II and III) valence bands.

majority of electron states of the supercell are not perturbed by the defect, and their contributions to dDOS will cancel out, which simplifies the analysis.

Before exploring the calculated dDOS for various defects, let us review the total DOS and site-projected DOS of the pristine TiC plotted in Fig. 1; the latter would be the reference DOS, term  $n_{0,s}$  in Eq. (1), for an infinitely large supercell. As has been shown previously [20,62,63], three typical energy regions in the band structure of TiC can be identified: region I (also referred to as the lower valence band), the states below  $-9$  eV, which are dominated by C- $2s$  states; region II (bonding part of the upper valence band), showing strong peaks due to hybridization between Ti- $3d$  and C- $2p$  states below the  $E_F$ ; as well as region III (antibonding part of the upper valence band) showing the strong hybridization peaks above the  $E_F$ . In region II, the most prominent Ti-C hybridization peak is situated around  $-2.5$  eV. In region III, the antibonding peaks due to Ti-C hybridization are situated around  $+4$  eV. Between the bonding and the antibonding peaks lies a valley of low DOS (dominated by Ti states) at around the  $E_F$ , sometimes also called a pseudogap. The lower and the upper valence bands (regions I and II) are separated by a full gap where electron states are forbidden in a perfect TiC crystal.

Let us classify the defects in TiC into two groups, according to the deviation from the stoichiometric composition that they cause. The first group (C-depleting defects) includes defects that produce concentration changes leading to substoichiometric  $Ti_{1-c}C_c$  ( $c < 0.5$ ), e.g., carbon vacancy  $Va_C$  and titanium interstitial  $Ti_I$ , together with its dumbbell conformations  $Ti_D$  and titanium antisite defect  $Ti_C$ . The other group (C-enriching defects) includes defects that produce concentration changes leading to superstoichiometric  $Ti_{1+c}C_c$  ( $c > 0.5$ ), e.g., titanium vacancy  $Va_{Ti}$ , several conformations of carbon interstitial  $C_I$ , including dumbbells  $C_D$ , and carbon antisite defect  $C_{Ti}$ . The calculated atomic and electronic structure is presented in Fig. 2

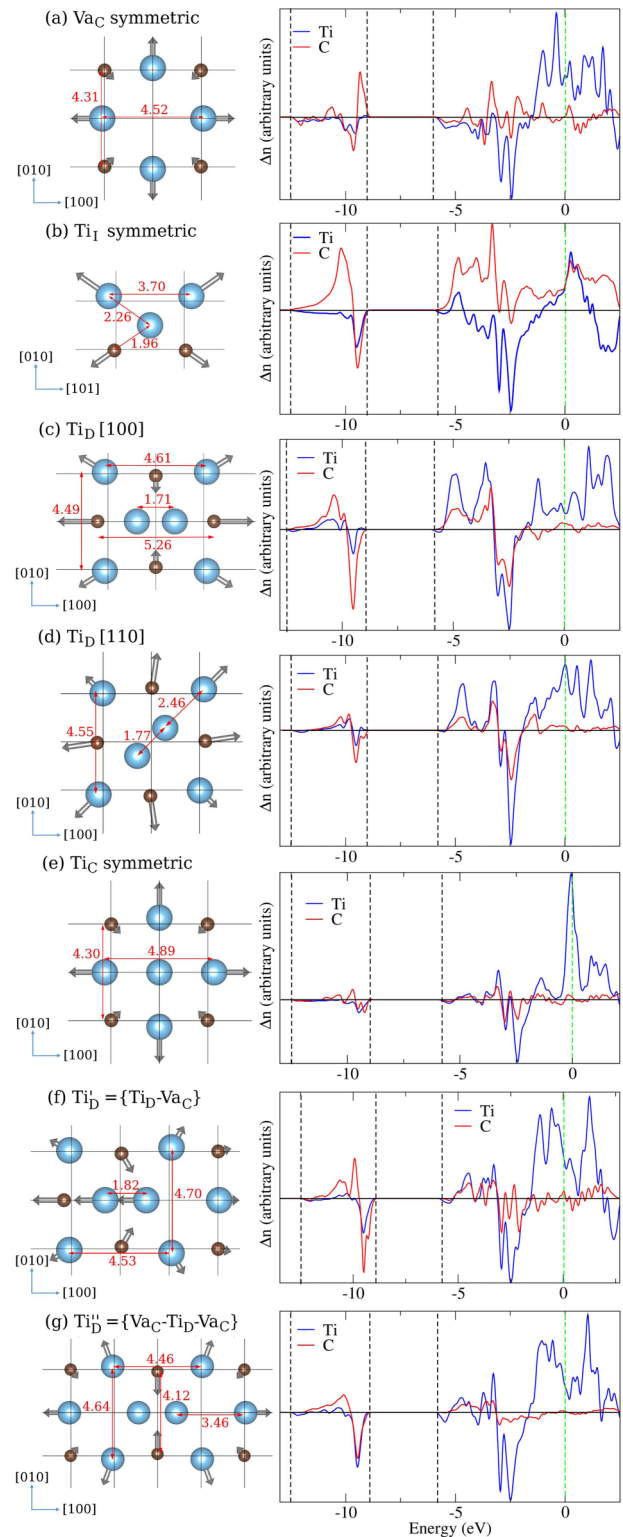


FIG. 2. (Color online) Computed atomic and electronic structure of C-depleting point defects in TiC. The blue and brown balls represent the Ti and C atoms, respectively. Gray arrows show the direction and magnitude (exaggerated) of the atomic displacements around the defect. Interatomic distances are indicated by numbers ( $\text{\AA}$ ) and red arrows. Vertical and horizontal thin lines show the positions of lattice planes in the perfect TiC. In dDOS plots, the vertical dashed lines indicate the band edges (green) and the Fermi level (dOS) as in Fig. 1, and the horizontal line indicates the zero level of dDOS.

for the C-depleting defects and in Fig. 3 for the C-enriching defects. See, Supplemental Material Ref. [64].

### A. C-depleting defects

Figure 2(a) shows the atomic relaxation pattern around a carbon vacancy  $Va_C$  which is the most abundant point defect in the C-poor TiC. In agreement with previous studies [40,42], we find that the distance between two Ti atoms along [100] is increased from 4.33 Å in the pristine TiC to 4.52 Å near the vacancy, while the distance between two C atoms is shortened to 4.31 Å. The corresponding dDOS,  $\Delta n$ , exhibits depletion of the host states near the hybridization peak at  $-2.5$  eV and creation of defect states in the pseudogap region around the  $E_F$ . As Fig. 2 shows, these dDOS features are exhibited not only by carbon vacancies, but by all the C-depleting defects. The electronic structure changes produced by C-depleting defects may, therefore, be described as a reduction in covalency and an enhancement in metallicity of the interatomic bonding in TiC. Another common feature exhibited by point defects of the C-depleting group is that they affect the electron states just inside the valence bands; no defect states are created in the forbidden energy regions.

The symmetric  $Ti_I$ , whose structure is shown in Fig. 2(b), turns out to be the stablest conformation of a titanium interstitial. Its split conformations  $Ti_D[100]$  and  $Ti_D[110]$  shown in Figs. 2(c) and 2(d) are found to be mechanically stable, but higher in energy than  $Ti_I$  by, respectively, 0.17 and 0.52 eV. The  $Ti_D[111]$  dumbbell orientation (not shown in Fig. 2) is even higher in energy, by 0.7 eV relative to  $Ti_I$ , and is mechanically unstable. The calculated dDOS for the symmetric conformation of  $Ti_I$  shows a through at  $-2.5$  eV and a peak of Ti states in the pseudogap around the  $E_F$ . In addition to these dDOS features, all the titanium dumbbell conformations produce characteristic defect states in the upper valence band at  $-3$  and at  $-5$  eV. These peaks can be attributed to the shorter Ti-C interatomic distance around the defects in comparison with the Ti-C distance in a perfect TiC lattice. The shorter Ti-C bonds for the Ti dumbbell conformations also explain the calculated redistribution of the DOS around  $-10$  eV in the lower valence band.

In the symmetric conformation of an antisite Ti defect (a Ti atom occupying a carbon site,  $Ti_C$ ) the surrounding Ti atoms are forced to move away from the center, while the neighboring C atoms are attracted to it. Its electronic structure, exhibiting a very sharp peak at the Fermi level, is typical of an unstable atomic configuration. Indeed, the symmetric conformation shown in Fig. 2(e) is mechanically unstable with respect to an off-center  $\langle 100 \rangle$  displacement of the antisite Ti atom to form a “split antisite” conformation  $Ti'_D$  shown in Fig. 2(f), which can be viewed as a  $Ti[100]$  dumbbell bound to a carbon vacancy, i.e., as a  $\{Ti_D-Va_C\}$  cluster. The asymmetric distortion of  $Ti_C$  splits up the sharp dDOS peak into bonding and antibonding peaks situated, respectively, below and above the  $E_F$ , thereby stabilizing split antisite  $Ti'_D$  conformation.

Furthermore, our calculations show that, in the presence of nearby carbon vacancies, both  $Ti_C$  and  $Ti_I$  can undergo a spontaneous transformation into the [100] dumbbell conformation, thereby producing a linear defect cluster  $\{Va_C-Ti_D-Va_C\}$

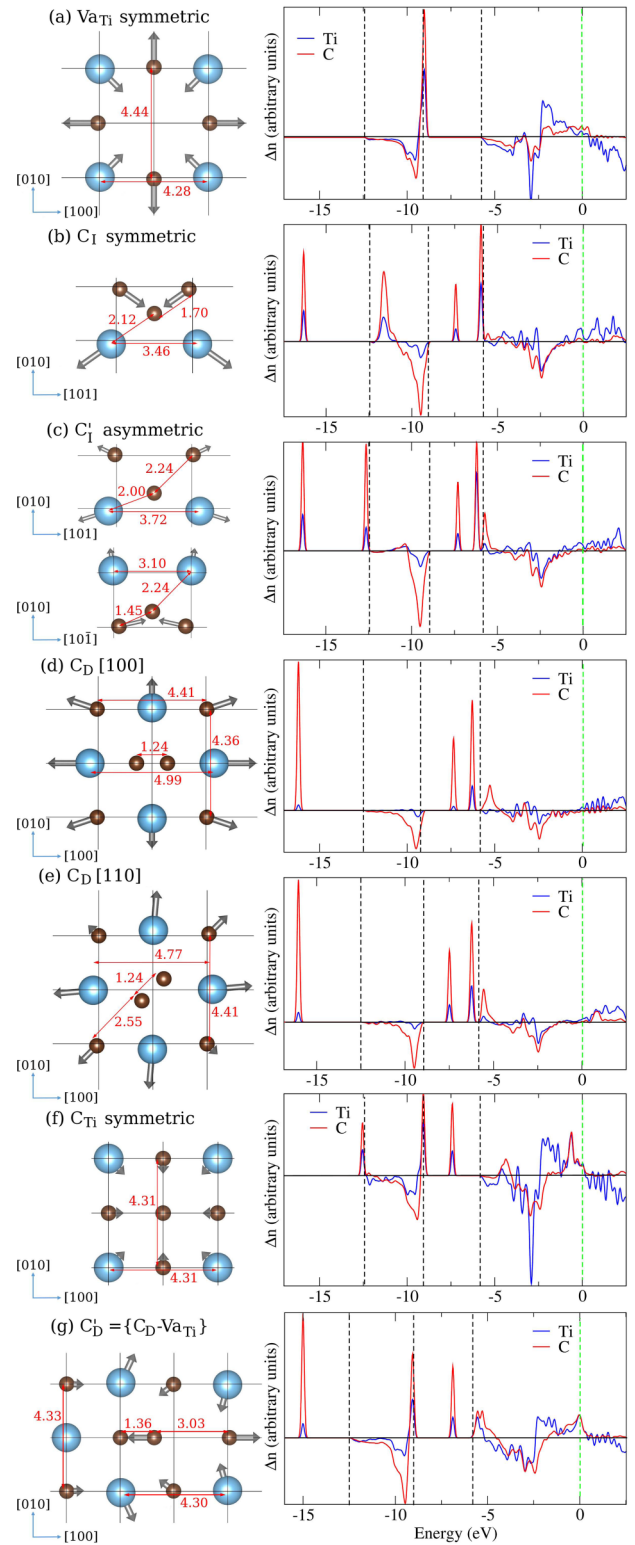


FIG. 3. (Color online) Computed atomic and electronic structure of C-enriching point defects in TiC. The blue and brown balls represent the Ti and C atoms, respectively. Gray arrows show the direction and magnitude (exaggerated) of the atomic displacements around the defect. Interatomic distances are indicated by numbers (Å) and red arrows. Vertical and horizontal thin lines show the positions of lattice planes in the perfect TiC. In dDOS plots, the vertical dashed lines indicate the band edges and Fermi level (green), as in Fig. 1, and the horizontal line indicates the zero level of dDOS.

shown in Fig. 2(g). As discussed in Sec. IV, the cluster is very stable. Due to its low symmetry, the defect states of this cluster are spread over a wider energy range inside the pseudogap as compared to the symmetric  $\text{Ti}_C$  or  $\text{Ti}_I$  conformations. It is noteworthy that the length of the dumbbell inside the cluster, 1.88 Å, is slightly larger than the Ti-Ti distance in the [100] dumbbell without the vacancies. Because of the two vacant carbon sites, the dDOS of the cluster shows a depletion of the bonding host states at  $-2.5$  eV, without any extra hybridization peaks in the range from  $-5$  to  $-2.5$  eV, in contrast to the dDOS of a vacancy-free  $\text{Ti}_D[100]$  dumbbell.

### B. C-enriching defects

Let us now analyze the atomic and electronic structure of C-enriching point defects in TiC that are presented in Fig. 3. Unlike  $\text{Va}_C$ , a titanium vacancy  $\text{Va}_{\text{Ti}}$  does not produce any defect states in the pseudogap around the  $E_F$ , but depletes the host states near the hybridization peaks at  $-2.5$  and  $-10$  eV. A very narrow defect state is created at the top of the lower valence band, which can be used for the detection of  $\text{Va}_{\text{Ti}}$ .

Figures 3(b)–3(e) show four different conformations of interstitial carbon that have been considered in our calculations: symmetric  $C_I$  (mechanically unstable), asymmetric  $C'_I$ , and two dumbbell conformations,  $C_D[100]$  and  $C_D[110]$ . These forms of interstitial carbon produce characteristic defect states in the forbidden energy regions (in the full gap separating the lower and upper valence band, as well as under the lower valence band). The defect states in the gap have prevalingly C-2p character, with a strong admixture of Ti states. The defect states under the lower valence band are almost entirely of C-2s character. These states originate from the covalent exchange interactions between the C atoms that occur at short distances (1.2–1.7 Å) from one another in these defect conformations. The number, character, and energy positions of the defect states depend on the number, symmetry, and length of the C-C bonds in the defect structures. The fact that these defect states do not overlap in energy with the host electron states allows for the detection and analysis of carbon interstitials and dumbbells using spectroscopic methods.

The electronic structure of a carbon antisite defect  $C_{\text{Ti}}$ , Fig. 3(f), is quite different from that of carbon interstitials. Due to the geometry of  $C_{\text{Ti}}$  with six relatively long ( $>2$  Å) C-C bonds, the antisite defect just broadens the lower valence band without producing any defect states under it. However, a distinct defect level is formed in the middle of the full gap at  $-7.5$  eV. Similar to titanium antisite, the symmetric  $C_{\text{Ti}}$  is unstable against a symmetry-breaking distortion into the split antisite  $C'_D = \{C_D\text{-Va}_{\text{Ti}}\}$  conformation. The dDOS of the split carbon antisite exhibits a peak under the lower valence band, at  $-15$  eV, which is characteristic of a longer C-C bond of 1.36 Å in the split antisite  $C'_D$  as compared to the C-C bond of only 1.24 Å in the carbon dumbbell  $C_D$ . This feature allows one to distinguish a split carbon antisite from carbon interstitials or dumbbells that typically produce deeper defect levels under the lower valence band.

## IV. DEFECT FORMATION ENERGIES

### A. Assumptions and definitions

Formally, the total energy of a defected crystal can be represented as the sum

$$E_{\text{tot}} = E_0 + \sum_i E_i^{\text{form}} + \frac{1}{2} \sum_{i,j} E_{i,j}^{\text{pair}} + \dots, \quad (2)$$

where the first term is the energy of the defect-free crystal, the second term is the sum of formation energies for all the defects that are present in the system, the third term is the sum of interactions for all pairs of the defects, etc. Thus, defect formation energy is defined as the excess energy due to the presence of a single, isolated defect of a certain kind in the crystal.

It should be noted here that the present analysis is based on total energies of the supercells that have been relaxed using methods of molecular statics, where all the ions are located at positions of zero force. We further discriminate between a (meta)stable defect conformation corresponding to a local minimum and an unstable conformation corresponding to a saddle point. All dynamical (phonon) contributions, starting from the zero-point energy term, are omitted in the present work. In general, these contributions are important for point-defect energetics [65], but their analysis is computationally very demanding. Previously it has been checked that the phonon contributions to the formation and interaction energies of Schottky pairs in TiC are of the order of 0.1 eV, i.e., at least 10 times as small as the static ion contributions [49].

In compounds, single-point defects (even native defects such as vacancies, interstitials, or antisites) alter the composition of the system, making the defect formation energy dependent on the chemical potentials of those atomic species whose numbers change when the defect is formed [65]. Alternatively, the defect formation energy may be defined as the energy of a certain “quasichemical” reaction having the defect as a product. The so-defined defect formation energy is naturally dependent on the energies of all the reactants and the products involved. On the other hand, defect formation energy may be interpreted as a thermodynamic property related to the (temperature dependence of) equilibrium defect concentration. In compounds, the equilibrium defect concentrations (as well as the quasichemical defect reactions that describe the equilibrium) depend not only on temperature, but also on the composition of the system (equivalently, on the chemical potentials). That is why, when a numerical value for a defect formation energy is given, the corresponding quasichemical reaction, chemical composition, or the chemical potentials must also be specified.

In semiconductors, the formation energy (together with the charge state) of an atomic defect additionally depends on doping of the host material or, equivalently, on the electron chemical potential (Fermi level) [65]. In metallic materials, defects are effectively screened from one another by the valence electrons of the host. To see any effect of doping, the dopant concentration in a metal should be comparable to the valence electron concentration. That is why the cohesive properties of metallic alloys and compounds mostly exhibit linear concentration dependencies, even at large defect

concentrations of a few percent. Eventual nonlinearities may be caused by the defect interactions as well as by concentration dependence of the defect formation energy.

Quite expectedly, the energy of formation for  $\text{TiC}_{1-x}$  exhibits a nonlinear behavior as a function of vacancy concentration: An initial shallow decrease of the energy of formation turns into a rapid increase at a carbon vacancy site fraction of about  $x = 0.1$  [44]. This effect can partly be attributed to the repulsive interactions among the carbon vacancies which strongly avoid each other at short (first- and second-nearest neighbor) distances on the carbon FCC sublattice [43,44,49]. Much stronger (and attractive) interactions have been found between the two different kinds of vacancies in TiC. Strong interactions stabilize associates, such as the  $\{\text{Va}_{\text{Ti}}\text{-}6\text{Va}_{\text{C}}\}$  cluster found previously [49] or the  $\{\text{Va}_{\text{C}}\text{-Ti}_{\text{D}}\text{-Va}_{\text{C}}\}$  cluster identified in this work, relative to dissociated arrangements of the point defects. Such associates can be treated as “molecular” species, each contributing to the total energy of the system with a certain formation energy according to Eq. (2). Individual point defects, as well as their associates, may exist in different spatial conformations. For example, an interstitial atom may occupy a symmetric (tetrahedral) interstitial site, be situated asymmetrically next to it, or form a dumbbell with a neighboring atom around a regular lattice site (so-called “split interstitial” conformation). Furthermore, several dumbbell orientations with respect to the crystal axes may be mechanically stable.

Here we restrict our consideration to small defect concentrations, corresponding to one or two point defects per 216-site supercell used in this work. As found in some previous studies [42,49], the interactions of an isolated defect (or a compact defect cluster) in the 216-site TiC supercell with its periodic images are negligible (mainly due to the metallicity of TiC). At such small defect concentrations (site fractions of about 1%–2%) weak defect-defect interactions  $E_{i,j}^{\text{pair}}$  may also be neglected. Without the interaction terms, Eq. (2) becomes formally equivalent to the lattice gas model of Wagner and Schottky [66]. Strongly bound associates of point defects can still be taken into consideration in the lattice gas model as molecular species. Moreover, the list of gas species may be extended to include various possible conformations of point defects and their associates. Thus, the total energy is represented here as the following sum of formation energies of all the defects present in the system

$$E_{\text{tot}} = E_0 + \sum_{\alpha} E_{\alpha}^{\text{form}} N_{\alpha}, \quad (3)$$

where  $\alpha$  enumerates the lattice gas species (including isolated point defects, strongly bound clusters, and all their conformations) and  $N_{\alpha}$  is the number of defect species  $\alpha$ .

## B. Individual point defects

As individual point defects do not conserve the host composition, their formation energies should be considered in the grand-canonical ensemble, i.e., as quantities dependent on the chemical potentials of the titanium  $\text{Ti}_{\text{res}}$  and carbon  $\text{C}_{\text{res}}$  atoms in the reservoir that have to be exchanged with the  $\text{Ti}_{1-c}\text{C}_c$  crystal to form the defect. The origin of this dependence can be understood if one considers the defects as

products of certain quasichemical reactions, for example,



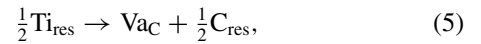
The energy of reaction Eq. (4) can be taken as the formation energy of a titanium antisite defect  $\text{Ti}_{\text{C}}$ . To write defect reactions, we follow a quasichemical convention in which the number of atoms (rather than the number of lattice sites) in the considered system is conserved [67–69]:

(1) atoms occupying regular lattice sites (e.g.,  $\text{C}_{\text{C}}$ ) are omitted;

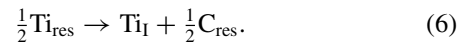
(2) the number of atoms in the system is conserved;

(3) the relative ratio of lattice sites between any two sublattices is fixed, while the total number of lattice sites can vary.

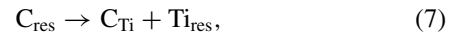
Under these conditions, the defect reaction to form a carbon vacancy in TiC reads as



while for a Ti interstitial one has



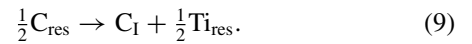
This list may be continued to include the defect reactions causing an excess of carbon by the formation of a carbon antisite,



a titanium vacancy



or a carbon interstitial defect



The energy of each defect reaction given by Eqs. (4)–(9) [the sum of energies for all the products minus the sum of energies for all the reactants] depends on the energies of titanium and carbon atoms in the reservoir,  $\mu(\text{Ti}) = \varepsilon(\text{Ti}_{\text{res}}) - \varepsilon_0(\text{Ti})$  and  $\mu(\text{C}) = \varepsilon(\text{C}_{\text{res}}) - \varepsilon_0(\text{C})$ ; the energies are expressed relative to the energies of standard states for the elements,  $\varepsilon_0(\text{Ti})$  and  $\varepsilon_0(\text{C})$ . Hereafter, the energy of a bulk system is denoted by  $\varepsilon$  if it is normalized per atom. Consequently, the formation energy for the corresponding point defect involves the value of the chemical potential  $\mu = \mu_{\text{C}} - \mu_{\text{Ti}}$  in the considered system. For refractory compounds like TiC, the dependence of chemical potential  $\mu(c)$  on the carbon concentration  $c$  is strong around the stoichiometric composition  $c = 0.5$ .

Figure 4 shows the energy of formation of  $\text{Ti}_{1-c}\text{C}_c$  compound,

$$\Delta\varepsilon_{\alpha}^{\text{form}} = \varepsilon(\text{Ti}_{1-c}\text{C}_c) - (1-c)\varepsilon_0(\text{Ti}) - c\varepsilon_0(\text{C}), \quad (10)$$

calculated for the stoichiometric TiC, as well as for nonstoichiometric supercells each containing a single point defect  $\alpha$  (vacancy, antisite, or interstitial) in its lowest-energy conformation. All the energies correspond to fully optimized geometries at zero pressure and are expressed per atom. The plot also includes the results for the supercell containing a  $\{\text{Va}_{\text{C}}\text{-Ti}_{\text{D}}\text{-Va}_{\text{C}}\}$  cluster, because, obviously, this defect cluster has a much lower energy than the individual point defects  $\text{Ti}_{\text{I}}$  or  $\text{Ti}_{\text{C}}$ . The arrows in the figure illustrate the fact that the

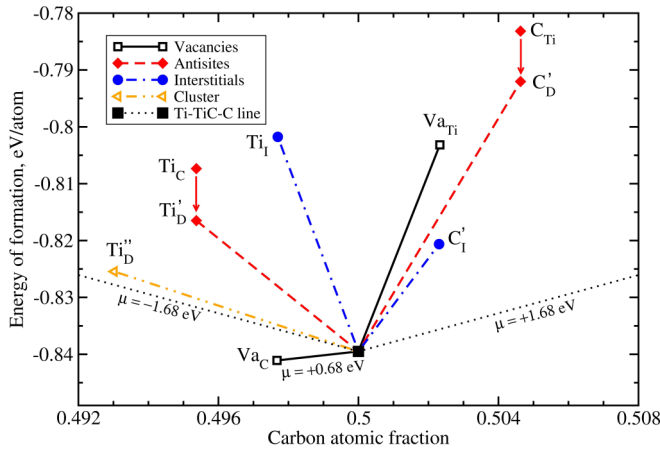


FIG. 4. (Color online) Energy of formation of the  $\text{Ti}_{1-c}\text{C}_c$  compound,  $\Delta\varepsilon^{\text{form}}$ , calculated as a function of carbon atomic fraction  $c$  in defect-free and defect-bearing supercells, relative to hcp titanium and diamond carbon (all energies are normalized per atom). The values of chemical potential  $\mu$ , corresponding to the slope of  $\Delta\varepsilon^{\text{form}}(c)$  in different regions of the Ti-C binary system, are indicated. Note that, for small concentration of carbon vacancies  $\text{Va}_C$ , the  $\mu$  is positive. It turns to negative values at much higher  $\text{Va}_C$  concentrations than those considered in the present work (see Ref. [44]).

symmetric antisite conformations  $\text{Ti}_C$  and  $\text{C}_{\text{Ti}}$  are unstable and spontaneously transform into the split antisite conformations (a  $\langle 100 \rangle$  dumbbell next to a vacancy). For a titanium antisite the transformation can be described as follows:  $\text{Ti}_C \rightarrow \text{Ti}'_{\text{D}} \equiv \{\text{Ti}_{\text{D}}\text{-Va}_C\}$ . A similar transformation occurs in the case of a carbon antisite,  $\text{C}_{\text{Ti}} \rightarrow \text{C}'_{\text{D}} \equiv \{\text{C}_{\text{D}}\text{-Va}_{\text{Ti}}\}$ . The defect formation energy is lowered by approximately 2 eV per defect in both cases.

For every defect species  $\alpha$ , the formation energy  $E_{\alpha}^{\text{form}}$  can be obtained from the corresponding linear dependence in Fig. 4 as

$$E_{\alpha}^{\text{form}} = \left( \frac{d\Delta\varepsilon_{\alpha}^{\text{form}}}{dc} - \mu \right) \frac{dc}{dn_{\alpha}}, \quad (11)$$

where  $n_{\alpha} = N_{\alpha}/N_{\text{at}}$  is the concentration of defect species  $\alpha$ , relative to the total number of atoms  $N_{\text{at}}$ , in the supercell. Depending on the composition, the value of the chemical potential (slope of the the lowest-energy “branch” of concentration dependence or that of the common tangent inside a two-phase region) in the Ti-C system may vary between two limits, from  $\mu \approx -2\Delta\varepsilon_0^{\text{form}}$  (two-phase mixture Ti-TiC) to  $\mu \approx +2\Delta\varepsilon_0^{\text{form}}$  (two-phase mixture TiC-C), that is, by about four times the energy of formation of the stoichiometric TiC compound  $\Delta\varepsilon_0^{\text{form}}$  (expressed per atom) [46]. The value  $\Delta\varepsilon_0^{\text{form}} = -0.84$  eV/atom calculated here for the stoichiometric TiC (relative to hcp Ti and diamond C) coincides with the value obtained previously using the same method [44] and is less negative than the standard value  $-0.934$  eV obtained by Frisk as a result of thermodynamic assessment [12]. (The energy difference between the diamond and graphite structures of carbon,  $\sim 0.0053$  eV/atom [70], is small compared to energies of our interest here.)

The calculated defect formation energies (including stable as well as some unstable conformations of point defects)

are presented in Table I, where the dependence on the chemical potential is indicated formally (in the first data column) as well as by providing the values of  $E_{\alpha}^{\text{form}}$  specific of C-poor ( $c < 0.5$ ,  $\mu = +0.68$  eV) and C-rich ( $c > 0.5$ ,  $\mu = +1.68$  eV) compositions. It should be emphasized that the calculated defect formation energies are applicable to  $\text{Ti}_{1-c}\text{C}_c$  at small deviations from the stoichiometric composition, most reliably within the interval  $0.49 \leq c \leq 0.51$ . Transferring the calculated defect energies to largely nonstoichiometric compositions (reaching  $c \approx 0.3$  in titanium carbide) is invalid without taking into account the strong concentration dependence of the energy of formation of C-poor  $\text{Ti}_{1-c}\text{C}_c$  [44], which is not considered here.

### C. Constitutional and thermal point defects

Our calculations reproduce the well-known fact that carbon vacancies  $\text{Va}_C$  (also referred to as structural vacancies) are constitutional defects in C-poor  $\text{Ti}_{1-c}\text{C}_c$ . As Fig. 4 shows, the  $\text{Va}_C$  branch of concentration dependence lies below the line representing the energy of the Ti-TiC phase mixture. Accordingly, the formation energy of  $\text{Va}_C$  is zero for C-poor compositions ( $c < 0.5$ ). The second in energy are asymmetric carbon interstitials  $\text{C}'_{\text{I}}$ , but their formation energy is not low enough to stabilize  $\text{Ti}_{1-c}\text{C}_c$  at C-rich compositions ( $c > 0.5$ ): The branch of  $\Delta\varepsilon_{\alpha}^{\text{form}}(c)$  corresponding to  $\alpha = \text{C}'_{\text{I}}$  lies above the TiC-C common tangent line. Next in energy, for the considered concentration range of  $\text{Ti}_{1-c}\text{C}_c$ , is  $\text{Ti}''_{\text{D}}$  cluster of a titanium dumbbell with two carbon vacancies. The formation energies of other point defects listed in Table I are so high that, on their scale, even the effect of the chemical potential appears to be rather weak.

Within the lattice gas model given by Eq. (3), the dependence on chemical potential completely cancels out if one considers certain composition-conserving combinations of point defects (where the individual defects are not associated into clusters). Table II shows some simple examples of such combinations. The corresponding defect reactions and formation energies have been obtained by combining the respective data of Eqs. (4)–(9) and Table I. Conservation of composition enables such defect combinations to form as thermal excitations in a closed system.

Let us make a qualitative analysis of thermal defects in TiC, assuming smallness of the defect concentrations. It has been shown [69,71] that the primary thermal defects are the lowest-energy composition-conserving combinations that involve two types of point defects. Table II shows that a Frenkel C pair (a carbon vacancy and an interstitial carbon atom) is, by far, the lowest-energy composition-conserving combination in TiC,  $E_{\text{FC}} = 3.75$  eV. At temperatures that are small compared to  $E_{\text{FC}}/2k_{\text{B}}$ , these Frenkel pairs are expected to be the dominant thermal defects in the whole concentration range of  $\text{Ti}_{1-c}\text{C}_c$  considered here.

#### 1. Nearly stoichiometric TiC

If the fraction of constitutional vacancies  $x_0$  in  $\text{TiC}_{1-x_0}$  is so small (or the temperature  $T$  is so high) that  $x_0 \ll 2 \exp(-E_{\text{FC}}/2k_{\text{B}}T)$ , the equilibrium concentration of thermally formed carbon vacancies and interstitials,  $x_{\text{thrm}}$ , exhibits

TABLE I. Computed formation energies (eV) of isolated point defects in  $\text{Ti}_{1-c}\text{C}_c$  and their dependence on the chemical potential around the stoichiometric composition ( $0.49 \leq c \leq 0.51$ ).

Defect species $\alpha$		Formation energy $E_{\alpha}^{\text{form}}$ (eV) for compositions in the range		
Notation	Conformation	$0.49 \leq c \leq 0.51$	$c < 0.5$	$c > 0.5$
C-depleting defects				
$\text{Va}_{\text{C}}$	Symmetric	$-0.34 + \mu/2$	0.00	0.50
$\text{Ti}'_{\text{D}}$	{ $\text{Va}_{\text{C}}\text{-Ti}_{\text{D}}\text{-Va}_{\text{C}}$ } cluster	$3.02 + 3\mu/2$	4.04	5.51
$\text{Ti}'_{\text{D}}$	{ $\text{Ti}_{\text{D}}\text{-Va}_{\text{C}}$ }, split antisite	$4.97 + \mu$	5.65	6.65
$\text{Ti}_{\text{C}}$	Symmetric, unstable	$6.94 + \mu$	7.62	8.62
$\text{Ti}_{\text{I}}$	Symmetric	$8.19 + \mu/2$	8.53	9.03
$\text{Ti}_{\text{D}}$	[100]	$8.36 + \mu/2$	8.70	9.20
$\text{Ti}_{\text{D}}$	[110]	$8.71 + \mu/2$	9.05	9.55
C-enriching defects				
$\text{C}'_{\text{I}}$	Asymmetric	$4.09 - \mu/2$	3.75	3.25
$\text{C}_{\text{I}}$	Symmetric, unstable	$4.53 - \mu/2$	4.19	3.69
$\text{C}_{\text{D}}$	[100]	$5.64 - \mu/2$	5.30	4.80
$\text{C}_{\text{D}}$	[110]	$6.32 - \mu/2$	5.98	5.48
$\text{Va}_{\text{Ti}}$	Symmetric	$7.81 - \mu/2$	7.47	6.97
$\text{C}'_{\text{D}}$	{ $\text{C}_{\text{D}}\text{-Va}_{\text{Ti}}$ }, split antisite	$10.25 - \mu$	9.57	8.57
$\text{C}_{\text{Ti}}$	Symmetric antisite, unstable	$12.17 - \mu$	11.49	10.49

an Arrhenius temperature dependence

$$x_{\text{thrm}} \approx \exp(-E_{\text{FC}}/2k_{\text{B}}T), \quad (12)$$

with an activation energy that is half of the formation energy of a Frenkel C pair, some 1.88 eV. Here  $k_{\text{B}}T$  is the Boltzmann constant.

## 2. Slightly C-poor TiC

If the fraction of constitutional vacancies is large (or the temperature is low) so that  $x_0 \gg 2 \exp(-E_{\text{FC}}/2k_{\text{B}}T)$ , the concentration of thermally formed Frenkel C pairs still exhibits an Arrhenius temperature dependence,

$$x_{\text{thrm}}x_0 \approx \exp(-E_{\text{FC}}/k_{\text{B}}T), \quad (13)$$

TABLE II. Computed formation energies (eV) of selected composition-conserving combinations of point defects in the stoichiometric and slightly off-stoichiometric TiC.

Name	Notation	Defect reaction	$E^{\text{form}}$
All compositions of $\text{Ti}_{1-c}\text{C}_c$ , $0.49 \leq c \leq 0.51$			
Frenkel C pair <sup>a</sup>	FC	$0 \rightarrow \text{Va}_{\text{C}} + \text{C}'_{\text{I}}$	3.75
Schottky defect (divacancy)	VV	$0 \rightarrow \text{Va}_{\text{Ti}} + \text{Va}_{\text{C}}$	7.47
Di-interstitial pair <sup>b</sup>	II	$0 \rightarrow \text{Ti}_{\text{I}} + \text{C}'_{\text{I}}$	12.28
Exchange antisite pair <sup>c</sup>	XA	$0 \rightarrow \text{Ti}'_{\text{D}} + \text{C}'_{\text{D}}$	15.22
Frenkel Ti pair	FT	$0 \rightarrow \text{Va}_{\text{Ti}} + \text{Ti}_{\text{I}}$	16.00
C-poor compositions, $c < 0.5$			
Interbranch $\text{Ti}''_{\text{D}}$	VDV	$3\text{Va}_{\text{C}} \rightarrow \{\text{Va}_{\text{C}}\text{-Ti}_{\text{D}}\text{-Va}_{\text{C}}\}$	4.04
Interbranch $\text{Ti}'_{\text{D}}$	DV	$2\text{Va}_{\text{C}} \rightarrow \{\text{Ti}_{\text{D}}\text{-Va}_{\text{C}}\}$	5.65
Interbranch $\text{Ti}_{\text{I}}$	TI	$\text{Va}_{\text{C}} \rightarrow \text{Ti}_{\text{I}}$	8.53
Interbranch $\text{Ti}_{\text{D}}$	TD	$\text{Va}_{\text{C}} \rightarrow \text{Ti}_{\text{D}}$	8.70
C-rich compositions, $c > 0.5$			
Interbranch $\text{C}'_{\text{D}}$	CT	$2\text{C}'_{\text{I}} \rightarrow \{\text{C}_{\text{D}}\text{-Va}_{\text{Ti}}\}$	2.07
Interbranch $\text{Va}_{\text{Ti}}$	VT	$\text{C}'_{\text{I}} \rightarrow \text{Va}_{\text{Ti}}$	3.72

<sup>a</sup>Interstitial  $\text{C}'_{\text{I}}$  in the asymmetric conformation.

<sup>b</sup>Interstitial  $\text{Ti}_{\text{I}}$  is in the symmetric tetrahedral site.

<sup>c</sup>Split antisite conformations  $\text{Ti}'_{\text{D}} = \{\text{Ti}_{\text{D}}\text{-Va}_{\text{C}}\}$  and  $\text{C}'_{\text{D}} = \{\text{C}_{\text{D}}\text{-Va}_{\text{Ti}}\}$ .

It should be noted that, at the exact stoichiometric composition, primary thermal disorder must appear in the form of composition-conserving defect combinations involving *positive* numbers of point defects. This constraint is not necessary for primary thermal defects at nonstoichiometric compositions or for secondary thermal defects (at any composition) because, in those cases, certain point defects are present in the system prior to the formation of new thermal defects. Therefore, the formation of new defects may be accompanied by the disappearance of preexisting defects. The corresponding defect reaction will then contain the preexisting defect species on the left-hand side.

Such thermal defects have been termed “interbranch defects” because they can be viewed as vertical transitions from the lowest-energy branch to a higher-energy branch of concentration dependence; the branches are shown as lines in Fig. 4. Table II gives sample reactions of such kind in which constitutional  $Va_C$  or primary thermal  $C'_1$  defects are annihilated to form other point defects in TiC.

The formation energies of titanium vacancies and interstitials (including their dumbbell and cluster conformations) are important for understanding the mechanism(s) of self-diffusion of metal atoms in strong compounds like TM carbides and nitrides [47,49,72–74]. The formation energy of the Frenkel Ti pair, as one component of the activation energy, reaches 16.00 eV, which is already much higher than the experimental total activation energy of Ti self-diffusion in TiC, 7.66 eV [72]. Although the calculated formation energy of a Schottky pair is close to the experimental activation energy, the contribution from the migration barrier, some 3.90 eV according to Ref. [47], must not be forgotten. With this component taken into account, the total activation energy of Ti self-diffusion via the Schottky Ti pair becomes much higher than the experimental value. Consequently, the Schottky or Frenkel Ti pairs can be excluded from the list of possible mediators of Ti atom self-diffusion in TiC.

Alternatively, titanium vacancies and interstitials may form by annihilating, respectively, carbon interstitials and carbon vacancies, that is, as interbranch defects (see Table II). The formation energies of  $Va_{Ti}$  and  $Ti_I$  via the interbranch defect reactions are much lower than the formation energies of the same defects as parts of the Schottky and Frenkel C pairs. However, the effective formation energy of a titanium interstitial from a carbon vacancy, 8.53 eV, is again too high. It is noteworthy that the formation energies of Ti interstitials and dumbbells for C-poor compositions (fourth column in Table I) are, in fact, the energies of corresponding composition-conserving reactions listed in Table II for this compositional region.

The formation energy of a titanium vacancy from a carbon interstitial is just 3.72 eV. However, the preexisting defect of this reaction ( $C'_1$ ) is not a constitutional defect by itself, but has to form thermally as a part of a Frenkel C pair. Therefore, in the whole compositional region except the very narrow near-stoichiometric region, the effective formation energy of a titanium vacancy ( $E_{FC} + E_{VT}$ ) is still 7.47 eV, the same as that of a Schottky defect. Table II also shows that single titanium interstitials or dumbbells (formed as interbranch defects) have formation energies in TiC comparable to that of single titanium vacancies.

It is thus clear that the mechanism of Ti self-diffusion in TiC is not mediated by single point defects but must involve more complex defect species. In a recent work it was reported that a strong attractive interaction with constitutional vacancies can lower the formation energy of a titanium vacancy in C-poor TiC down to about 3 eV, which indicates that vacancy clusters rather than single metal vacancies may be mediators of metal diffusion in refractory carbides [49]. The formation energies of dumbbell–vacancy clusters  $Ti'_D$ ,  $Ti_D$ , and  $C'_D$  obtained in this work are also quite low (see Table II) and may be compatible with the activation energy of Ti self-diffusion in TiC. It remains to be investigated whether the migration of such clusters or Ti interstitials can be a feasible mechanism of Ti self-diffusion in TiC. We hope to address this problem in a separate publication.

## V. CONCLUSIONS

Titanium carbide is a naturally substoichiometric compound which is known to contain carbon vacancies as constitutional defects. Very little has been known about other point defects in TiC. In this work the geometry, electronic structure, and formation energies of various types and conformations of point defects in TiC are investigated by means of *ab initio* calculations. Asymmetric conformations of C-depleting and C-enriching defects have been sought by displacing some atoms from the symmetric positions and letting the structure fully relax. The tendency of C-depleting defects, such as titanium interstitials and antisites, to form clusters with carbon vacancies (the most abundant defects at C-rich compositions) has also been considered in the calculations.

The following defect species have been identified as mechanically stable point defects in C-poor TiC (in the order of increasing energy): carbon vacancy  $Va_C$ , [100] titanium dumbbell terminated by two carbon vacancies  $Ti'_D$ , [100] titanium dumbbell terminated by one carbon vacancy  $Ti_D$  (split Ti antisite), interstitial titanium  $Ti_I$  occupying a symmetric tetrahedral position, and titanium dumbbell  $Ti_D$  in the [100] and [110] orientations. Carbon vacancies are obtained to be the constitutional defect in C-poor TiC, in agreement with experimental observations.

Our calculations predict C-rich TiC compositions to be thermodynamically unstable relative to the stoichiometric TiC and pure carbon (no constitutional C-enriching defects), in agreement with the Ti-C phase diagram. The following C-enriching defect species are obtained to be mechanically stable: asymmetric carbon interstitial  $C'_1$ , carbon dumbbell terminated by a titanium vacancy  $C'_D$  (split C antisite), and titanium vacancy  $Va_{Ti}$ .

The electronic structure of all these stable (as well as of some unstable) defect conformations has been calculated and presented in the form of dDOS exhibiting positive peaks at the energies of defect states and negative peaks at energies of annihilated host states due to the defect formation. For the C-depleting defects the electronic structure changes occur inside the upper valence band, near the pseudogap centered at  $E_F$  (defect states) and near the Ti-C bonding peak at  $-2.5$  eV (annihilated host states). The C-enriching defects are found to produce characteristic defect states in the forbidden energy regions: inside the full gap separating the lower and

the upper valence bands (between  $-9$  and  $-6$  eV), as well as under the lower valence band (at  $-15$  eV and below). The position of these defect levels in the forbidden energy regions allows for the detection and identification of carbon interstitials, dumbbells, and split antisites in TiC by spectroscopic methods.

A qualitative analysis of the defect chemistry in TiC is given in the lattice gas model of Wagner and Schottky using the calculated energies of the defect species. The primary thermal defects for all studied compositions where  $Ti_{1-c}C_c$  is stable are found to be Frenkel C pairs, each involving a carbon vacancy and an asymmetric carbon interstitial. In the C-poor region of TiC, other C-depleting defects may form as interbranch defects, by annihilating constitutional carbon vacancies. The formation energies of vacancy-terminated and isolated titanium dumbbells  $Ti'_D$ ,  $Ti'_D$ , and  $Ti_D$  are in the range

that makes these defects suitable candidates for mediators of Ti self-diffusion in titanium carbide.

### ACKNOWLEDGMENTS

Authors thank Vsevolod Razumovskiy, Maxim Popov, and an anonymous reviewer for critical reading of the manuscript and making valuable comments. This work has been performed within the VINNEX center Hero-m, financed by the Swedish Governmental Agency for Innovation Systems (VINNOVA), Sweden, Swedish industry, and the KTH-Royal Institute of Technology, Stockholm, Sweden. We are grateful to the Swedish National Infrastructure for Computing (SNIC), Sweden and MATTER Network for computational resources at the National Supercomputer Center (NSC), Linköping, Sweden. W.S. acknowledges Olle Eriksson at Uppsala University for his support on the usage of computational time.

- 
- [1] W. S. Williams, *Science* **152**, 34 (1966).
- [2] L. E. Toth, *Transition Metal Carbides and Nitrides* (Academic Press, New York, 1971).
- [3] H. O. Pierson, *Handbook of Refractory Carbides and Nitrides: Properties, Characteristics and Applications* (William Andrew, Westwood, NJ, 1996).
- [4] P. H. Mayrhofer, C. Mitterer, L. Hultman, and H. Clemens, *Progr. Mater. Sci.* **51**, 1032 (2006).
- [5] Edited by O. T. Sorenson, *Nonstoichiometric Oxides* (Academic Press, New York, 1981).
- [6] Edited by L. Mandelcorn, *Non-stoichiometric Compounds* (Academic Press, New York, 1981).
- [7] Edited by R. Freer, *The Physics and Chemistry of Carbides, Nitrides, and Borides* (Kluwer, Dordrecht, 1990).
- [8] K. Kosuge, *Chemistry of Nonstoichiometric Compounds* (Oxford University Press, Oxford, 1994).
- [9] A. I. Gusev, A. A. Rempel, and A. J. Magerl, *Disorder and Order in Strongly Nonstoichiometric Compounds: Transition Metal Carbides, Nitrides and Oxides* (Springer, Berlin, 2001).
- [10] S. V. Didziulis and K. D. Butcher, *Coord. Chem. Rev.* **257**, 93 (2013).
- [11] J. Billingham, P. S. Bell, and M. H. Lewis, *Acta Crystallogr. A* **28**, 602 (1972).
- [12] K. Frisk, *CALPHAD: Comput. Coupling Phase Diagrams Thermochem.* **27**, 367 (2003).
- [13] K. Schwarz, *CRC Crit. Rev. Solid State Mater. Sci.* **13**, 211 (1987).
- [14] V. A. Gubanov, A. L. Ivanovsky, and V. P. Zhukov, *Electronic Structure of Refractory Carbides and Nitrides* (Cambridge University Press, Cambridge, UK, 1994).
- [15] A. H. Cottrell, *Chemical Bonding in Transition Metal Carbides* (Institute of Materials, London, 1995).
- [16] E. I. Isaev, S. I. Simak, I. A. Abrikosov, R. Ahuja, Yu. Kh. Vekilov, M. I. Katsnelson, A. I. Lichtenstein, and B. Johansson, *J. Appl. Phys.* **101**, 123519 (2007).
- [17] D. G. Pettifor, B. Seiser, E. R. Margine, A. N. Kolmogorov, and R. Drautz, *Philos. Mag.* **93**, 3907 (2013).
- [18] P. Blaha and K. Schwarz, *Int. J. Quantum Chem.* **23**, 1535 (1983).
- [19] V. P. Zhukov and V. A. Gubanov, *J. Phys. Chem. Solids* **46**, 1111 (1985).
- [20] D. L. Price and B. R. Cooper, *Phys. Rev. B* **39**, 4945 (1989).
- [21] J. Häglund, A. Fernández Guillermet, G. Grimvall, and M. Körling, *Phys. Rev. B* **48**, 11685 (1993).
- [22] R. Ahuja, O. Eriksson, J. M. Wills, and B. Johansson, *Phys. Rev. B* **53**, 3072 (1996).
- [23] A. J. Scott, R. Brydson, M. MacKenzie, and A. J. Craven, *Phys. Rev. B* **63**, 245105 (2001).
- [24] J. Redinger, R. Eibler, P. Herzig, A. Neckel, R. Podloucky, and E. Wimmer, *J. Phys. Chem. Solids* **46**, 383 (1985).
- [25] P. Marksteiner, P. Weinberger, A. Neckel, R. Zeller, and P. H. Dederichs, *Phys. Rev. B* **33**, 812 (1986).
- [26] A. L. Ivanovsky, V. I. Anisimov, D. L. Novikov, A. I. Lichtenstein, and V. A. Gubanov, *J. Phys. Chem. Solids* **49**, 465 (1988).
- [27] W. S. Williams, *Mater. Sci. Eng. A* **105–106**, 1 (1988).
- [28] M. Guemmaz, A. Mosser, and J. C. Parlebas, *J. Electron Spectrosc. Relat. Phenom.* **107**, 91 (2000).
- [29] L. I. Johansson, L. A. Hagström, B. E. Jacobson, and S. B. M. Hagström, *J. Electron Spectrosc. Relat. Phenom.* **10**, 259 (1977).
- [30] A. L. Ivanovsky, V. A. Gubanov, G. P. Shveikin, and E. Z. Kurmaev, *J. Less-Common Met.* **78**, 1 (1981).
- [31] A. Dunand, H. D. Flack, and K. Yvon, *Phys. Rev. B* **31**, 2299 (1985).
- [32] V. N. Lipatnikov, L. V. Zueva, A. I. Gusev, and A. Kottar, *Phys. Solid State* **40**, 1211 (1998).
- [33] L. V. Zueva and A. I. Gusev, *Phys. Solid State* **41**, 1032 (1999).
- [34] V. Moisy-Maurice, N. Lorenzelli, C. H. de Novion, and P. Convert, *Acta Metall.* **30**, 1769 (1982).
- [35] C. H. de Novion and J. P. Landesman, *Pure Appl. Chem.* **57**, 1391 (1985).
- [36] T. Priem, B. Beuneu, C. H. de Novion, J. Chevrier, F. Livet, A. Finel, and S. Lefebvre, *Phys. B (Amsterdam, Neth.)* **156–157**, 47 (1989).
- [37] G. Brauer, W. Anwand, E. M. Nicht, P. G. Coleman, A. P. Knights, H. Schut, G. Kogel, and N. Wagner, *J. Phys.: Condens. Matter* **7**, 9091 (1995).
- [38] M.-P. Delplancke-Ogletree and O. R. Monteiro, *J. Vac. Sci. Technol.* **15**, 1943 (1997).
- [39] G. Li and L. F. Xia, *Thin Solid Films* **396**, 16 (2001).

- [40] K. E. Tan, A. M. Bratkovsky, R. M. Harris, A. P. Horsfield, D. Nguyen-Manh, D. G. Pettifor *et al.*, *Modell. Simul. Mater. Sci. Eng.* **5**, 187 (1997).
- [41] E. R. Margine, A. N. Kolmogorov, M. Reese, M. Mrovec, C. Elsässer, B. Meyer, R. Drautz, and D. G. Pettifor, *Phys. Rev. B* **84**, 155120 (2011).
- [42] H. W. Hugosson, P. Korzhavyi, U. Jansson, B. Johansson, and O. Eriksson, *Phys. Rev. B* **63**, 165116 (2001).
- [43] P. A. Korzhavyi, L. V. Pourovskii, H. W. Hugosson, A. V. Ruban, and B. Johansson, *Phys. Rev. Lett.* **88**, 015505 (2002).
- [44] D. A. Andersson, P. A. Korzhavyi, and B. Johansson, *CALPHAD: Comput. Coupling Phase Diagrams Thermochem.* **32**, 543 (2008).
- [45] S. H. Jhi, S. G. Louie, M. L. Cohen, and J. Ihm, *Phys. Rev. Lett.* **86**, 3348 (2001).
- [46] H. M. Pinto, J. Coutinho, M. M. D. Ramos, F. Vaz, and L. Marques, *Mater. Sci. Eng., B* **165**, 194 (2009).
- [47] V. I. Razumovskiy, P. A. Korzhavyi, and A. V. Ruban, *Solid State Phenom.* **172–174**, 990 (2011).
- [48] L. Tsetseris, S. Logothetidis, and S. T. Pantelides, *Acta Mater.* **56**, 2864 (2008).
- [49] V. I. Razumovskiy, A. V. Ruban, J. Odqvist, and P. A. Korzhavyi, *Phys. Rev. B* **87**, 054203 (2013).
- [50] P. Hohenberg and W. Kohn, *Phys. Rev.* **136**, B864 (1964).
- [51] W. Kohn and L. J. Sham, *Phys. Rev.* **140**, A1133 (1965).
- [52] P. E. Blöchl, *Phys. Rev. B* **50**, 17953 (1994).
- [53] G. Kresse and D. Joubert, *Phys. Rev. B* **59**, 1758 (1999).
- [54] G. Kresse and J. Hafner, *Phys. Rev. B* **48**, 13115 (1993).
- [55] G. Kresse and J. Hafner, *Phys. Rev. B* **49**, 14251 (1994).
- [56] G. Kresse and J. Furthmüller, *Phys. Rev. B* **54**, 11169 (1996).
- [57] J. P. Perdew, K. Burke, and M. Ernzerhof, *Phys. Rev. Lett.* **77**, 3865 (1996).
- [58] M. Methfessel and A. T. Paxton, *Phys. Rev. B* **40**, 3616 (1989).
- [59] K. Momma and F. Izumi, *J. Appl. Cryst.* **44**, 1272 (2011).
- [60] P. A. Korzhavyi and R. Sandström, *Comput. Mater. Sci.* **84**, 122 (2014).
- [61] A. Laio and F. L. Gervasio, *Rep. Prog. Phys.* **71**, 126601 (2008).
- [62] Seung-Hoon Jhi and Jisoon Ihm, *Phys. Rev. B* **56**, 13826 (1997).
- [63] Z. Dridi, B. Bouhafs, P. Ruterana, and H. Aourag, *J. Phys.: Condens. Matter* **14**, 10237 (2002).
- [64] See Supplemental Material at <http://link.aps.org/supplemental/10.1103/PhysRevB.91.134111> for more detailed structural information.
- [65] C. Freysoldt, B. Grabowski, T. Hickel, J. Neugebauer, G. Kresse, A. Janotti, and C. G. Van de Walle, *Rev. Mod. Phys.* **86**, 253 (2014).
- [66] C. Wagner and W. Schottky, *Z. Phys. Chem., Abt. B* **11**, 163 (1930).
- [67] There are several (equivalent) conventions to write defect reactions; see Ref. [68] for a review and Ref. [69] for an application example of the presently used convention that is better adapted to model thermal or irradiation-induced defects in a closed system.
- [68] H. Wenzl, W. A. Oates, and K. Mika, Defect thermodynamics and phase diagrams in compound crystal growth processes, in *Handbook of Crystal Growth: Fundamentals, Part A: Thermodynamics and Kinetics*, edited by D. T. J. Hurle (Elsevier, Amsterdam, 1993), Vol. 1, pp. 105–186.
- [69] P. A. Korzhavyi, A. V. Ruban, A. Y. Lozovoi, Yu. Kh. Vekilov, I. A. Abrikosov, and B. Johansson, *Phys. Rev. B* **61**, 6003 (2000).
- [70] A. Dinsdale, *CALPHAD: Comput. Coupling Phase Diagrams Thermochem.* **15**, 317 (1991).
- [71] P. A. Korzhavyi, I. A. Abrikosov, and B. Johansson, *MRS Proc.* **552**, KK5.35.1 (1998).
- [72] S. Sarian, *J. Appl. Phys.* **40**, 3515 (1969).
- [73] R. A. Andrievskii, Yu. F. Khromov, and I. S. Alekseeva, *Fiz. Met. Metalloved.* **32**, 664 (1971).
- [74] R. A. Andrievskii, *Poroshk. Metall. (Kiev)* **50**, 5 (2011) [*Powder Metall. Met. Ceram.* **50**, 2 (2011)].